Multifractal Properties of Solar Magnetograms

N. G. MAKARENKO

Pulkovo Astronomical Observatory,
65/1, Pulkovo Highway
196140, St.Petersburg, Russia
E-mail: ng-makar@mail.ru

L. M. KARIMOVA

Institute of Mathematics,
125 Pushkin Street,
050010, Almaty, Kazakhstan
E-mail:klyailya@mail.ru

M. M. NOVAK

Faculty of CISM,
Kingston University,
Surrey KT1 2EE, UK
E-mail: novak@kingston.ac.uk

Abstract

We explore the multiscale properties of magnetic field distributions using magnetograms obtained from the Michelson Doppler Imager (MDI) on board the Solar and Heliospheric Observatory (SOHO). Multifractal spectra were estimated with the help of microcanonical formalism applying Choquet capacities. We have extracted spectra both for active regions (AR) and for regions outside of AR. It has been found that background field multifractal spectra are stable and do not change their forms during approximately 24 hours. The spectra of active regions are more changeable, but there is no evidence that their variability is associated with the onset of the flares. To verify the magnetic field multifractal scaling existence, we construct a toy model with three symbols, a version of the Chaos Game. The empirical measures and those of the toy model (obtained from the solution of inverse problem, by means of Iterated Functions System (IFS) with Markov random choice of the functions) were compared. As the constructed models provide a satisfactory fit to theoretical and empirical measures of toy models, we conclude that obtained scaling estimations of the magnetograms can really result from the multifractal properties of the solar magnetic field dynamics.

Preprint submitted to Elsevier Science *22 December 2008*

Key words: solar magnetic field, microcanonical multifractal formalism, Choquet capacity, Chaos game
PACS: 96.60Hv, 89.75Da, 95.75Mn

1 Introduction

The Sun's activity, with its strong influence on the weather, is a manifestation of nonlinear dynamics of solar magnetic fields [1]. The complexity of magnetic fields in solar plasmas is related to magnetohydrodynamic turbulence. The most frequently proposed solar dynamo mechanism, dealing with the generation of solar magnetic fields deep in the convection zone as well as the rise of magnetic flux tubes toward the atmosphere, involves *the Kolmogorov theory* of turbulence [1,2]. Actually, photospheric magnetism is controlled by the large magnetic *Reynolds number* ($R_m \sim 10^8$). For such large R_m numbers the field is highly intermittent, i.e., it possesses fully developed turbulence. The phenomenology of magnetohydrodynamic turbulence in the solar atmosphere suggests a hierarchical self-organization and statistical self-similarity (multifractality) of the observed magnetic structures. The turbulent interaction between the magnetic field and plasma [3,4] can, in particular, lead to the release of tremendous amounts of energy, which was stored in the magnetic field, and can produce instabilities, which drive Coronal Mass Ejection (CME) and solar flares. Thus, these events are the product of critical threshold in a turbulent magnetic configuration. Many investigations are devoted to finding this threshold in scaling and multiscaling spectra of the observed magnetograms (for example [3,5–10]). However, up to now, the main problem centres on obtaining reliable estimations of scaling.

To estimate the scaling, various approaches are used, *e.g.*, the perimeter-square relationship [10] and the generalized dimension [3] calculated with the help of measure moments or by means of structure functions [7,9]. One can find a comparative analysis of obtained results concerning flare forecasting[8,2]. It should be mentioned that numerical variants of multifractal formalism are developed in detail for time series. Direct translation of this formalism [11] to digital images, representing magnetograms, generates difficulties associated with choosing a measure and discrete character (discontinuities) of the digital image. Normally, the image is considered as a hilly surface, whose 'elevation' is proportional to a gray level or digital value. However, erratic sum of gray levels does not help with the estimation of stable scaling exponent [3,8]. So, it is more reasonable to apply local estimation of singular measure instead of statistical one. In this work we apply the microcanonical multifractal formalism [12] and the method adapted to digital images that is based on Choquet capacities [13]. The latter is a generalization of Borel measures: they do not

satisfy the additivity condition, but preserve the feature of monotony for a sequence of nested sets. The goal of this paper is to establish and estimate multifractal spectra of the Michelson Doppler Imager (MDI) data of the solar magnetic field. We aim to answer two questions. The first one is whether the statistical scale invariance exists in the radial component of the intensity of the magnetic field. And the second one is to establish if there is a difference in the scaling characteristics between the active regions and the quieter background field. To verify the existence of multifractal features of solar magnetic field, we construct the *toy model* of the random (*Markov*) dynamical system (RDS), realized with the help of *Iterated Function System* (IFS) on a compact set. For this purpose image matrix is converted to a one dimensional array. Then the investigated time series is transformed into symbolic sequences according to a chosen rule.

The IFS system has a unique invariant multifractal measure. Histograms of magnetic field values of different fragments of MDI magnetograms are used to transform the gray levels into symbolic sequences. Then, with the help of the Chaos Game algorithm, an empirical measure is estimated and used to solve inverse problem of IFS [14–16]. The probabilities thus found are applied in RDS. Then with the help of cumulative histograms we show that model's and empirical measures coincide in a frame of toy models, that points to the reality of multifractal properties of the solar magnetic field.

The paper is structured as follows. Sec. 2 describes briefly a microcanonical formalism. In Sec. 3 we outline the multifractal analysis of images, based on the *Choquet capacities*. Then, in Sec. 4, we represent the obtained multifractal spectra of MDI magnetograms. Sec. 5 is devoted to the verification of the multifractal scaling. Mathematical details of some concepts in geometric measure theory can be found in the Appendix.

2 Microcanonical Multifractal Formalism

2.1 Brief review of measure theory

Let us recall that the *Lebesgue measure* $\mathcal{L}(A)$ of a set $A \in R^n$ is a way of assigning to A a number, which corresponds to the 'size' of the set. One may consider an infinite mass uniformly distributed over R^n such that the mass in any unit n-cube is one. The Lebesgue measure $\mathcal{L}(A)$ of A is the 'amount of matter in A'. In particular, $0 \leq \mathcal{L}(A) \leq \infty$. If $\mathcal{L}(A) < \infty$ for a bounded set A, then measure is called the *Radon* measure.

It is difficult to assign 'size' to an arbitrary set, commonly, a class of *Borel sets*,

$\mathcal{B} = \{B_i\}$, is chosen in R^n. Recall that the set $A \in X \subset R^n$ is *open* if every point in A has a neighborhood lying in the set, i.e., starting from any point $x \in A$ one can move by a small amount in any direction and still be in the set A. The set C is *closed* if the complement of C in X, i.e., $X - C$ is an open set. The Borel sets are the sets that can be constructed from open or closed sets by repeatedly taking countable unions and intersections: $\bigcup_{i=1}^{\infty} B_i \in \mathcal{B}$ and $\bigcap_{i=1}^{\infty} B_i \in \mathcal{B}$.

We call μ a measure on X if μ assigns a non-negative number, possibly ∞, to each subset $B_i \in \mathcal{B}$. The *Borel* measure of a set $A \in X$, that can be represented as union of Borel sets, i.e. $A = \cup_{i=1}^{n} B_i$ with $B_i \cap B_j = \varnothing, i \neq j$ is defined with the help of condition of additivity $\mu(A) = \sum \mu(B_i)$. Thus when $B_i \in R^n$ are intervals of type $[a_i, b_i]; [a_i, b_i] \times [a_i, b_i]; ..., [a_i, b_i] \times [a_i, b_i] \times ...[a_i, b_i]$, then the Borel measure is simply the Lebesgue measure: lenght $|b_i - a_i|$, area $|b_i - a_i|^2$ or $n-$volume $|b_i - a_i|^n$.

An analog of length for the Borel set B is *diameter* $\mid B \mid = \sup\{|x - y|, x, y \in B\}$. Let $A \in \cup_{i=1}^{\infty} B_i$ and $|B_i| \leq \delta$ for all i. Then value

$$H_{\delta}^{s}(A) = \lim_{\delta \to 0} inf \sum_{i=1}^{\infty} |B_i|^s \tag{1}$$

is called the s-dimensional *Hausdorff measure*, where $infimum$ is taken from all countable covers of the set A. Thus, the Hausdorff measure of a set A may be equal to $0, \infty$ or any intervening number. There exists a value s which can be a noninteger, so that $H^{s'}(A) = 0$ for any $s' > s$ and $H^{s'}(A) = \infty$ for all $s' < s$. Such value s is called the *Hausdorff dimension* of the set A.

2.2 The Multifractal measures

Measure, as 'mass distributions' in R^n, can be nonuniform. It can concentrate in points, intervals, areas etc. and its 'density' can change randomly. Let $\mu(B_x(r))$ be the value of mass in a ball of size r centered at point x. It is possible that density $\rho = \triangle\mu/\triangle r$, where $\triangle\mu = \mu(B_x(r + \triangle r)) - \mu(B_x(r))$ is not limited when $\triangle r \to 0$. Such measure is called *singular* with *singularity strength*, or the Hölder exponent, of $h(x)$. The value h is estimated by two conditions: $\Delta\mu/|\Delta r|^{\beta} = 0$ if $\beta < h$ and $\Delta\mu/|\Delta r|^{\beta} = +\infty$ if $\beta > h$. Class of measures satisfying local law

$$\mu(B_x(\epsilon)) \sim \epsilon^{h(x)} \tag{2}$$

is called the *Hausdorff measures*. It is clear that power law (2) exhibits the feature of *scale invariance*.

Let us select subsets $A_h \in A$, that have fixed value h, on a measure support ($supp\ \mu$) and will use A_h dimension as a "size". For this purpose we cover each element of the subset A_h by balls of size ϵ. The number of such balls, $N_h(\epsilon)$, for a given h, behaves like [12,17]

$$N_h(\epsilon) \sim \epsilon^{-f(h)}. \tag{3}$$

Subsets A_h can be a set of points, compact area or fractal. So $f(h)$ is generally the Hausdorff dimension

$$f(h) = d_H\{x \in supp\ \mu |\ h(x) = h\}. \tag{4}$$

Thus each element from collection A_h describes measure distribution on separate fractal component. All components together combine into a *multifractal* [17–19].

2.3 The Microcanonical formalism

A plot $(h, f(h))$ is called a *multifractal spectrum.* The $h(x)$ describes the singularity strength of the measure μ at the point x and is often called the *Hölder exponent* of the measure. The smaller the exponent $h(x)$, the more singular the measure around x and the stronger the singularity. The corresponding singularity spectrum, $f(h)$, often, but not always, is a convex curve with $f''(h) < 0$ for all h [17]. For example, the so called Legendre spectrum has always convex form [11], but a large deviation spectrum [17] can have multimodal form for a set of different multifractal measures.

There are two approaches for numerical estimation of a multifractal spectrum. In a frame of traditional, so called *canonical multifractal* formalism, spectra are estimated statistically by means of scale averaging-out of measure statistical moments [11,20,18]. Microcanonical formalism, on the other hand, estimates exponents $h(x)$ on a local scale, geometrically [12,21,22], as a slope of log-log linear regression at a point x in equation (2). In this latter case, the measure is estimated inside a small ball, $B_x(\epsilon)$, of size ϵ centered at x,

$$\mu(B_x(\epsilon)) = \int\limits_{y \in B_x(\epsilon)} d\mu(y). \tag{5}$$

Then, an appropriate operator is applied to extract the scale dependence. The operator applied to μ produces a new function $T_r\mu$ that assigns singularity exponent $h(x)$ to each point x, when the following condition is true [21,22]

$$T_r\mu = a_x r^{h(x)} + O(r^{h(x)}), \tag{6}$$

where $O(r^{h(x)})$ denotes members of sequence having high order infinitesimals. In a simple variant, T_r corresponds to a linear increment $|\Delta_r \mu|$ of the signal

$$T_r \mu = |\Delta_r \mu| = |\mu(x+r) - \mu(x)| \approx r^{h(x)}. \tag{7}$$

The histogram method estimation of the multifractal spectrum (see equation (3)) is based on statistical interpretation of the spectrum, namely, probability, $Prob_r(h)$, of observing a singularity h at r scale behaving as [17]

$$Prob_r(h) \propto r^{d-f(h)}, \tag{8}$$

where d is the topological dimension of the support μ.

It is considered that the measure μ is multifractal in a frame of microcanonical formalism, if there is T_r such that equation (5) holds true [21,22]. The histogram method estimates a large deviation spectrum and, as a rule, obtained curve does not have a smooth form [12], contrary to the Legendre spectrum.

3 Multifractal Analysis of Images.

When dealing with multifractal analysis of images, values of *gray scale* are taken as providing the base information about the measure. Gray scale image in $2D$ space $I(\mathbf{x})$, $\mathbf{x} \in Z \times Z$ is represented as a map $I : R \times Z \times Z \to R$. Here, point $\mathbf{x}$ is determined by integer coordinates (x, y) on a grid of pixels $Z \times Z$, and $I(\mathbf{x})$ takes on a value from gray levels, usually as $I(\mathbf{x}) \in [0, 255]$. Sometimes, a contrast $C(\mathbf{x}) = I(\mathbf{x}) - < I(\mathbf{x}) >$ is used. Under the assumption that $C(\mathbf{x})$ is differentiable function and its gradient $| \bigtriangledown C|(\mathbf{x})$ is locally integrated, it is possible to define measure density as $d\mu = d\mathbf{x}| \bigtriangledown C|(x)$ [21,22]. Then image measure of small neighborhood $\mu(A)$ is represented by means of integral $\int_A d\mu(\mathbf{x})$.

The equation (2) for image measure is often represented in the form

$$\mu(B_{\mathbf{X}}(\epsilon)) \approx a(\mathbf{x}) \epsilon^{d+h(\mathbf{X})} \tag{9}$$

where $d = 2$ is image support dimension and $a(\mathbf{x})$ is a coefficient [21,22]. In a case when $log \mid \mu \mid / log \mid \epsilon \mid < 2$, negative values of exponents h can appear.

To avoid difficulties related to pixelization, one may use projection measure on an appropriate wavelet basis [12,21]. Unfortunately, for images with high

variability $I(\mathbf{x})$, there are obstacles to estimate correctly a gradient and, consequently, to get correct values of the exponents [23]. Actually, to obtain correct estimation for a gradient $\mid \bigtriangledown C\mid(\mathbf{x})$, a sequence of values

$$\frac{C(x+\epsilon_k)-C(x)}{\epsilon_k}, \frac{C(x+\epsilon_{k-1})-C(x)}{\epsilon_{k-1}}, ..., \frac{C(x+\epsilon_1)-C(x)}{\epsilon_1}$$

must become at least stable for a set of scales $\epsilon_1 < \epsilon_2 < \epsilon_3...$ near the smallest available image resolution ϵ_1, but this is not satisfied for highly variable data $I(x)$. Therefore, in this work we use the *Choquet capacity* as a measure. One may find full definitions in [13,23,24] and we provide a heuristic description in what follows.

Let E is a set and $\mathcal{P}$ is a set of subsets of E, which is closed relative to finite union and finite intersection. The function $c : \mathcal{P} \rightarrow R$ is called the *Choquet capacity*, when the following conditions of monotony are true [13,23,24]

- c is non decreasing: if $A \subseteq B$, then $c(A) \leq c(B)$.
- If $\{A_n\}$ is an increasing sequence of nested subsets, i.e. $A_i \subseteq A_{i+1}$, then:

$$c(\bigcup_n A_n) = \sup_n c(A_n).$$

- If $\{A_n\}$ is a decreasing sequence of subsets $\mathcal{P}$, i.e. $A_{i+1} \subseteq A_i$, then:

$$c(\bigcap_n A_n) = \inf_n c(A_n).$$

Let an image be defined on a unit square $E = [0,1]\times[0,1]$ and $\mathcal{P} = \{E_i\}, i \geq 1$ is a sequence of partitions E, where E_i consists of whole number of pixels. Let $I(x,y)$ be a gray level of the pixel (x,y) and Ω is an image object. We use the following two capacities [15]:

- *Max-capacity*: $c^M(\Omega) = \max_{x,y\in\Omega} I(x,y)$.
- *Iso-capacity*: $c^i(\Omega) = \max_l \sharp\{(x,y) \mid |I_c - I(x,y)| \leq l, (x,y) \in \Omega\}, l > 0$, where I_c is a gray level of central pixel of Ω and the symbol $\sharp$ denotes the "integer number of pixels".

Now we clarify these capacities. The Max-capacity, $c^M(\Omega)$, is the maximum value of the brightness of pixels in the image region Ω that depends on the gray level value only. The Iso-capacity, $c^i(\Omega)$, is a number of pixels in the region Ω with a brightness that can not be distinguished from central pixels up to l. According to the definition, the capacities are monotonous functions of the region size, contrary to photometrical *sum-measure*:

$$c^s(\Omega) = \sum_{(x,y)\in\Omega} I(x,y). \tag{10}$$

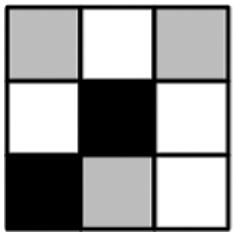

$$\begin{pmatrix} 25 & 0 & 27 \\ 0 & 255 & 0 \\ 254 & 25 & 0 \end{pmatrix}$$

Fig. 1. Image region and its matrix representation in gray scale.

The example in Fig. 1 illustrates the above-mentioned formal definitions. Left and right parts demonstrate image region Ω and their corresponding values $I(\mathbf{x})$. It is clear that $c^s(\Omega) = 586$ and $c^M(\Omega) = 255$. For $l = 2$ we get $c^i(\Omega) = 2$, that means existence of two pixels: $255, 254$ with $|I_c - I(\mathbf{x})| \leq 2$.

4 Multifractal Spectra of MDI magnetograms.

We used magnetograms of the total Solar disk obtained from Michelson Doppler Imager (MDI) instrument on board of the Solar and Heliospheric Observatory (SOHO). These are accessible in online archive [25] in fits-format. We have estimated multifractal large deviation spectra of solar magnetic field using "FracLab" software [26] and our own programs. Data presented for analysis are in matrixes consisting of 1024×1024 pixels, representing positive and negative values of solar magnetic field as gray level. Light color corresponds to positive polarity, whereas dark represents negative polarity. Solar Active Regions (AR) consist of spots of different polarity that are visible as dark and light clusters. To reveal features of scale invariance, 256×256 pixels fragments were chosen within AR (Fig.2) and from outside of AR (Fig.3), to investigate the AR and the background. Analyzed sample consisted of 46 magnetograms. Space resolution of magnetograms is $2''$, so analyzed fragments of the Sun have the area of $(37 * 10^4 \times 37 * 10^4) km^2$. Numerical analysis demonstrated that the most appropriate among the above-described capacities is Iso-capacity, which was applied in this investigation. Typical results are represented in figures below.

As a rule, multifractal spectra obtained for images outside of AR have smooth shape with long right tail, which in the majority of cases extends up to the Hölder exponent $h_{max} \approx 8$ (Fig.4). In a few fragments, however, the Hölder exponent is bounded to $h_{max} \approx 2$ (Fig.5). Background spectra are relatively stable, are practically independent of the selected fragment and have not changed during the time interval of 24 hours used for the analysis.

Multifractal spectra of the AR have a staircase-like form for the right-hand branch (Fig.6). This effect is the result of the existence of a few distinctive scales connected, perhaps, with the quantization step of the image. Put oth-

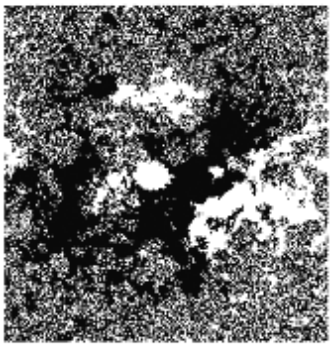

Fig. 2. The fragment consisting of AR.

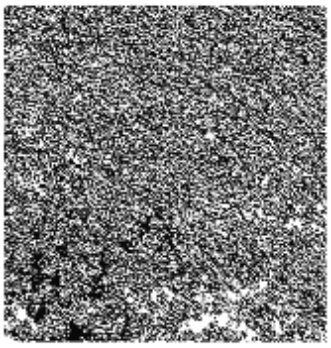

Fig. 3. The fragment of background field

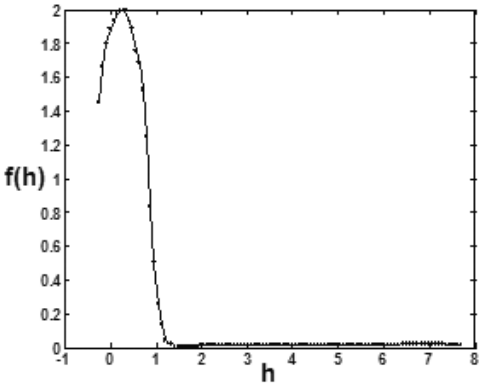

Fig. 4. Multifractal spectrum of background with long tail.

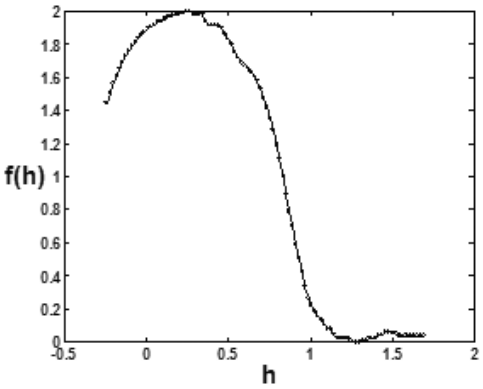

Fig. 5. Multifractal spectrum of background without long tail.

erwise, fluctuations in the gray levels are higher in the AR. Sometimes, the form of the AR spectrum changes and becomes smoother, and components with high value of the Hölder exponents appear in the right tail of spectrum (Fig.7). In many cases, significant changes in the spectra were observed for image fragments preceding the flares. However, we do not have sufficient evidence to claim that this is always the case, as sometimes the AR multifractal spectra change even in the absence of the flare (Fig.8).

5 Verification of the Multifractal Scaling Reality.

Experimental $f(\alpha)$-spectra confirm the existence of statistical self-similarity in photospheric magnetic fields. In this section we introduce additional arguments in support of the multifractal features of the magnetic field. For this purpose we apply a *toy model* as a random dynamical system (RDS) [27]. It

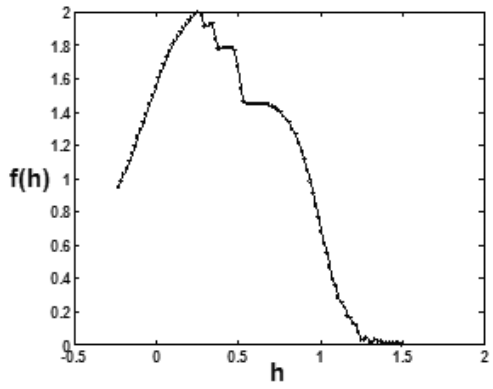

Fig. 6. Multifractal spectrum of AR before flare without long tail.

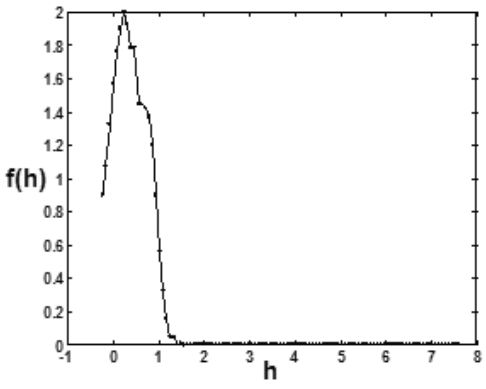

Fig. 7. Multifractal spectrum of AR before flare with long tail.

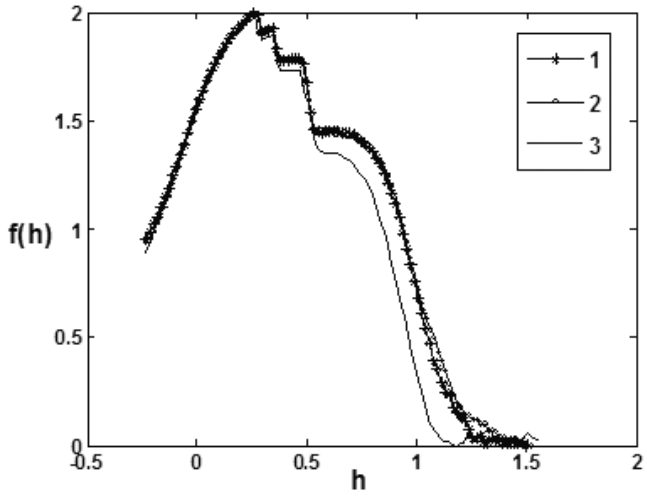

Fig. 8. Multifractal spectra for fragments of AR:
1 — before flare (07.06.2000); 2 — after flare ; 3 — without flare.

produces multifractal measures with characteristics that depend on a set of parameters. We choose these parameters based on statistics of the MDI information and show that model is fitting the MDI scaling features. More precisely, we took an Iterated Functions System (IFS) as a model basis [19]. The RDS is realized by independent or Markov random choice of the IFS functions. In the Markov case the RDS dynamics is defined by transition probabilities, which produce a unique invariant multifractal measure on the IFS attractor under iterations [19,14]. With an IFS, its attractor and its measure being given, the inverse problem is to find probabilities, which are free parameters of the model. This leads to an optimization problem with the distance between the theoretical invariant measure of the model and the empirical measure of the experimental data (or their moments) as a functional to be minimized [28]. If this problem is solved, then the IFS, with the found probabilities, acts as a

model that describes a multifractal structure of the data [19,28,29].

5.1 A brief theory of IFS

Let us consider a 1D metric space (R, d) with metric $d(x, y) = |x-y|; x, y \in R$ for simplicity. A finite set of affine mappings $\{w_i\}_{i=1}^N : w_i = c_i x + a_i$, such as $|w_i(x) - w_i(y)| \leq c|x - y|, c < 1$ is called an *Iterated (hyperbolic) Function System*(IFS). The *Hutchinson operator* is the mappings joint operation [19,30]

$$\mathbf{w} = \bigcup_{i=1}^{N} w_i. \tag{11}$$

Intervals can be considered as "points" in the space of compacts $\mathcal{H}$, which becomes metric with the help of the *Hausdorff distance* $d_H(A, B)$ (see Appendix). It can be easily proved [19,30] that

$$d_H(\mathbf{w}(A), \mathbf{w}(B)) \leq c d_H(A, B), \tag{12}$$

where the constant $c = \max\{c_i\}$ is the maximal contraction factor of the IFS. In other words, the Hutchinson operator is a contraction with the contraction factor c in the space $(\mathcal{H}, d_H)$. Then, according to *Banach's* contraction mapping theorem, $\mathbf{w}$ has a unique fixed point in $(\mathcal{H}, d_H)$. The point is in fact an invariant subset $\mathcal{A} \in \mathcal{H}(X)$ that satisfies $\mathcal{A} = \mathbf{w}(\mathcal{A})$ and is called an *attractor* of the IFS [19]. Moreover, for any $B \in \mathcal{H}(X)$, we have

$$\lim_{n\to\infty} \mathbf{w}^{\circ n}(B) \to \mathcal{A}, \tag{13}$$

where $\mathbf{w}^{\circ n}(B) = \mathbf{w}(\mathbf{w}^{\circ(n-1)}(B))$.

The convergence rate to the attractor is estimated by the *Collage Theorem* [30]: for any of $B \in \mathcal{H}(X)$ and IFS $\{w_i\}, i = 1, 2, .., N$ with the attractor $\mathcal{A} = \mathbf{w}(\mathcal{A})$, the following inequality holds

$$d_H(\mathcal{A}, B) \leq (1 - c)^{-1} d_H(B, \mathbf{w}(B)). \tag{14}$$

Let us consider an IFS $\{w_1, w_2\}$

$$w_1(x) = (1/2)x;\ w_2(x) = (1/2)x + (1/2). \tag{15}$$

with the unit segment $I = [0, 1]$ as its attractor. Assume, I supports the unit Borel measure $\mu(I) = 1$. Consider how the IFS works on the measure [14,29,30]. For this purpose choose the mappings w_i, $i = 1, 2$ from (13)

with probabilities $p_1 = 1/3; p_2 = 2/3$ respectively at each iteration $\mathbf{w}^{\circ n}, n \geq 1$. Then, after the first iteration w_1 the supporting segment will be twice contracted: $w_1(I) \to I_1 = [0, 1/2]$, and $(1/3)$ portion of the initial measure will be concentrated on I_1, i.e., $\mu(I_1) = (1/3)\mu(w_1^{-1}(I_1)$, where $w_1^{-1}(I_1)$ is a preimage of I_1, i.e., the initial segment I. The second mapping w_2 gives the right half of I: $w_2(I) \to I_2 = (1/2, 1]$ with measure $\mu(I_2) = (2/3)\mu(w_2^{-1}(I_2))$ on it. Both mappings $w_i, i = 1, 2$ work independently, but the initial measure mass remains, i.e.,

$$\mu(I) = p_1\mu(w_1^{-1}(I_1)) + p_2\mu(w_2^{-1}(I_2)) = p_1\mu(I) + p_2\mu(I), \tag{16}$$

where *push forward measure* $\mu(w_i^{-1}(B)) = w_i \circ \mu(B)$ denotes the image measure of the set B under w_i (see Appendix). The equation(16) declares the property of self-similarity and invariance of the measure [30]. The next iteration of the operator $\mathbf{w}^{\circ 2}$ will lead to simple "reweighing" of the original measure:

$$\mu(I) = p_1(p_1\mu(I) + p_2\mu(I)) + p_2(p_1\mu(I) + p_2\mu(I)). \tag{17}$$

By continuing this process, we will obtain a distribution of a so-called binomial measure [18].

By analogy with space $(\mathcal{H}, d_H)$, it is possible to consider space of Borel measures $(\mathcal{M}, d_M)$ with the *Monge-Kantorovich-Hutchinson metrics* $d_M(\mu, \nu)$(see Appendix). Let (X, d) be a compact metric space and $(\mathcal{M}, d_M)$ denotes the space of normalized Borel measures on X. Let $\{w_i; p_i\}, p_1 + ... + p_N = 1, p_i > 0$ be a hyperbolic IFS with probabilities. Then the *Markov operator* [19,30] associated with the IFS is the function $\mathbf{M} : \mathcal{M}(X) \to \mathcal{M}(X)$ defined by

$$\mathbf{M}(\mu) = \sum_{i=1}^{N} p_i\mu \circ w_i^{-1} \tag{18}$$

for all $\mu \in \mathcal{M}(X)$. The $\mathbf{M}$ is a contraction mapping in $(\mathcal{M}, d_M)$, with contractivity factor c with respect to metric d_M

$$d_M(\mathbf{M}(\mu), \mathbf{M}(\nu)) \leq sd_M(\mu, \nu) \tag{19}$$

It can be proved [19,30] that under sufficiently general assumptions, almost any IFS with probabilities has a unique invariant measure, so that for every Borel subset $A \in X$

$$\mu(A) = \mathbf{M}(A) \equiv \sum_{i=1}^{N} p_i\mu \circ w_i^{-1}(A) \tag{20}$$

supported by the attractor of the IFS. If μ is invariant measure then for every continuous function $f : X \to R$, the following relation holds

$$\int_X f(x)d\mu(x) = \sum_{i=1}^{N} p_i \int_X f \circ w_i(x)d\mu(x). \tag{21}$$

5.2 Random Dynamical System and Chaos Game

Now we demonstrate how to get invariant measure with the help of RDS. The unit segment I is an attractor of the IFS $\{w_1, w_2; p_1, p_2 = 1 - p_1\}$, defined by (15). Let $x_0 \in I$ be an initial point, then RDS, in a form of IFS with probabilities, generates a random orbit [27]

$$\{x_k\}_{k=0} : x_k = w_{\sigma_k} \circ w_{\sigma_{k-1}} \circ ... \circ w_{\sigma_1}(x_0), \tag{22}$$

where numbers of mappings $\sigma_i \in 1, 2$ are chosen according to given probabilities. If the probability of the current number in (22) depends on the previous one, $P(\sigma_i = i|\sigma_{i-1} = j) = p_{ij}$, then we have Markov case. Invariant measure of any interval $I_k \subset I$ is defined as a limit [19,30]

$$\mu(I_k) = \lim_{l\to\infty}(I_k \cap x_1, x_2, ..., x_l)/l \tag{23}$$

for almost any random orbit. In other words, invariant measure is just a relative duration of the iterated point in the interval. Let us assume that we somehow get an estimation of invariant measure. Then using equation (21) we have a possibility to reconstruct the RDS in a form of IFS with probabilities. This is all about an inverse problem in fractal theory [14–16].

How to obtain measure estimation? We transform random orbit (22) to a symbolic sequence $s = s_1 s_2 ...$ using, for example, symbols from the binary alphabet: $s_i \in \{0, 1\}$. By "reading" it with the help of a sliding window of length L, we will collect a set of binary words. It is obvious, that one can construct 2^L different words using L symbols. Each word $s_1 s_2 ... s_L$ has a binary expansion or "address" [30]

$$x = s_1/2 + s_2/2^2 + ... + s_l/2^L, \tag{24}$$

where $x \in [0, 1]$.

Then statistics of the words can be investigated with the help of a histogram of their address distribution among 2^L bins on I . This scheme can be eas-

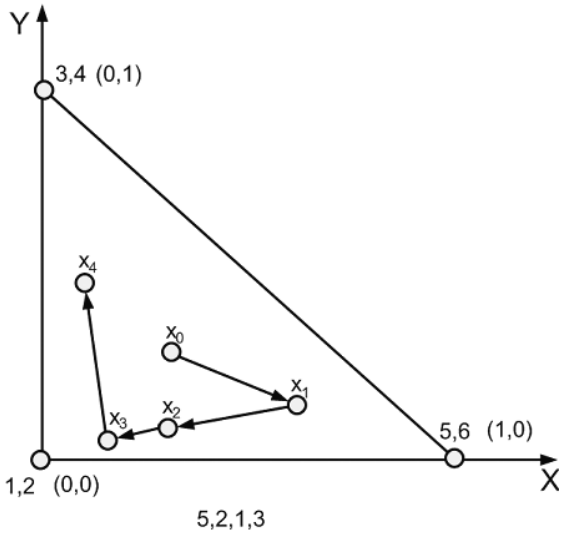

Fig. 9. Example of Chaos Game.

ily extended to $k-$symbols alphabet. In this case addresses are assigned by $k-$base expansion of words.

Our immediate task is to obtain empirical estimation of measure (23) for magnetograms, which are assumed to be produced by random dynamics (22), on the basis of IFS with probabilities. We apply the well-known Chaos Game, first suggested by Jeffrey [31] for visualization of geometrical structures of gene structure (DNA), in order to estimate the measure [29]. We use a 3-symbols version of the Game for reasons, which will be clarified further. The Game algorithm consists of the following steps (Fig.9):

(1) Consider a right angle triangle with vertices $\nu_1(0,0)$, $\nu_2(0,1)$, and $\nu_3(1,0)$ on plane (XY) and associate the first vertex ν_1 with a pair of numbers $(1,2)$, ν_2 with $(3,4)$ and ν_3 with $(5,6)$, respectively.
(2) Choose an arbitrary point, x_0, inside the triangle, and define its evolution by the random process, such as a successive tossing of a die.
(3) After the first toss, find a vertex with a corresponding number. For instance, number 5 corresponds to the pair $(5,6)$, i.e. vertex ν_3. Therefore, the point x_0 moves to the point x_1, which bisects the line segment $[x_0, \nu_3]$. The point x_1 becomes a new current point.
(4) Toss a die and repeat step 3, applying it to the current point.

Figure 9 shows an example of the Game having the sequence of numbers $5,2,1,3$. If the Game is governed by a symbolic sequence, consisting of 3 symbols s_1, s_2, s_3, the appearance of symbol s_i means application of the $i-th$ mapping.

Numeric experiments with the Chaos Game were carried out using sampled 256×256 pixels fragments of MDI-images of the background field and frag-

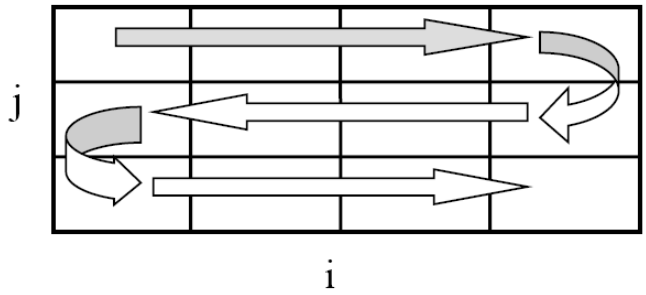

Fig. 10. Scheme of transforming matrix (m_{ij}) to a one dimensional array t: i is the column number, j is the row number.

ments of active areas. Every digital image matrix (m_{ij}) was preprocessed by increasing the value of its elements by the absolute value of the minimal element and then dividing them by their sum. Thus, sum of all the elements of the preprocessed matrix was equal to 1. After that the matrix was converted to a one dimensional array $\{t_i\}$, by connecting a successive row to previous one according to the scheme in Fig. 10.

As a result of preprocessing we obtained time series for the background field and for the active areas. Frequency histogram (Figure 11) was used to choose thresholds for symbolic transformation. We chose two threshold values: $h_1 = 1.50 \times 10^{-5}$ and $h_2 = 1.56 \times 10^{-5}$, which were boundaries of the range of maximal difference between background and AR data.

Then the investigated time series were transformed into symbolic sequences $s = (s_i), i = 1, 4, 9, .., n^2$ according to the following rule:

$$s_i = \begin{cases} 0, \text{ if } t_i < h_1; \\ 1, \text{ if } h_1 \leq t_i < h_2; \\ 2, \text{ if } t_i \geq h_2. \end{cases} \tag{25}$$

Thus, small normalized values were assigned a symbol 0, large values were assigned a 2, and symbol 1 corresponded to the values of the central part of the histogram. The obtained symbolic sequences governed the Chaos Game. Position of a current point x_i after the $(i+1)-$th iteration was defined by the following rule:

$$x_{i+1} = \begin{cases} (x_i + \nu_1)/2, \text{ if } s_i = 0; \\ (x_i + \nu_2)/2, \text{ if } s_i = 1; \\ (x_i + \nu_3)/2, \text{ if } s_i = 2. \end{cases} \tag{26}$$

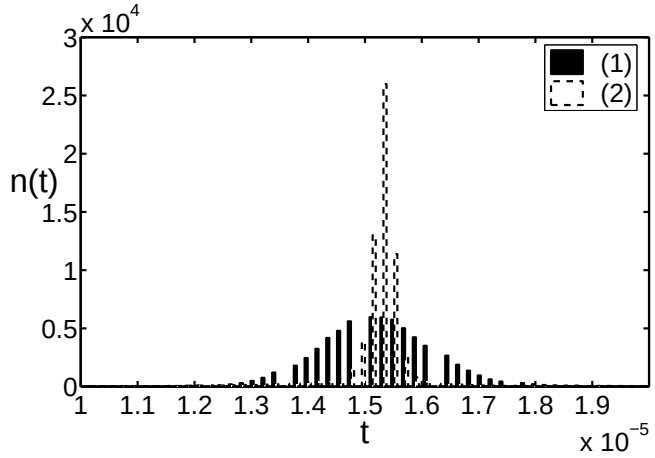

Fig. 11. Histograms of a one dimensional array $\{t_i\}$ for the background field (1) and an active region (2).

In order to obtain an empirical estimation of the measure (23), produced by RDS dynamics in a framework of the Chaos Game, the initial triangle on the plane was divided into boxes, and then relative amount of points inside each box was calculated.

Plots of $2D$ images of measures, corresponding to symbolic sequences for background field and active area, are given in the figures 12 and 13. In the case of background field, the measure support reproduces almost "uniform" Sierpinski triangle (Fig.12) that corresponds to chaotic symbolic sequence [31]. In the case of active area, the triangle is filled "non-uniformly", namely, a lot of points fall on the edge of the outer triangle (Fig. 13). It is necessary to emphasize that we do not deal here with the fractal Sierpinski triangle, but with a multifractal measure distributed throughout the background and active areas. It is clear that thus constructed toy model measures are not unique and depend on the number and levels of thresholds for symbolic transformation (25) and (26) .

The measures, obtained with the help of the toy model, were used for the solution of the inverse IFS problem, with the IFS defined by (26). We do not go into details here, as they can be found in [14,29,15,16]. Let us just summarize the main idea. The method exploits measure invariance property of eq. (21) adapted to the Markov model. A commonly used way to find a solution for the problem is to apply the method of moments [15,16], which minimizes the distance between moments of theoretical and empirical measures. Theoretical measure has transition probabilities, which are to be found by optimization. In this work we adopted another approach, based on the collage theorem (14) and L_1-metric [14]. The obtained transition probabilities were used to generate theoretical measure with the help of RDS. Theoretical and empirical measures were compared by means of cumulative histograms, analogous to those used

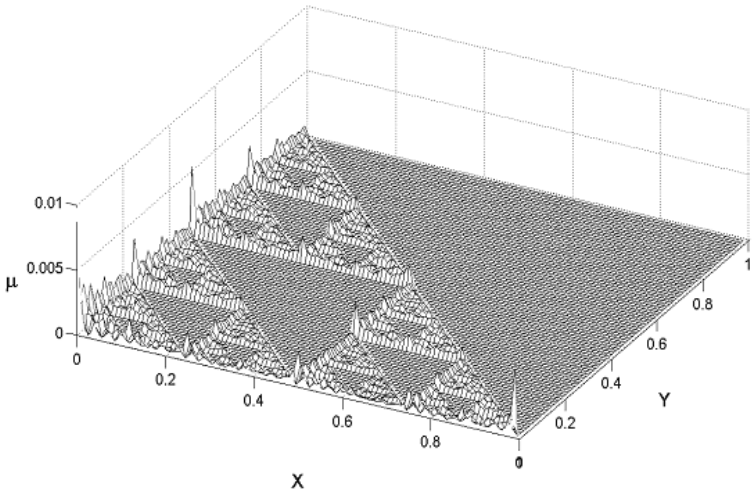

Fig. 12. Toy model measure for background field obtained by means of Chaos Game from empirical one dimensional array $\{t_i\}$.

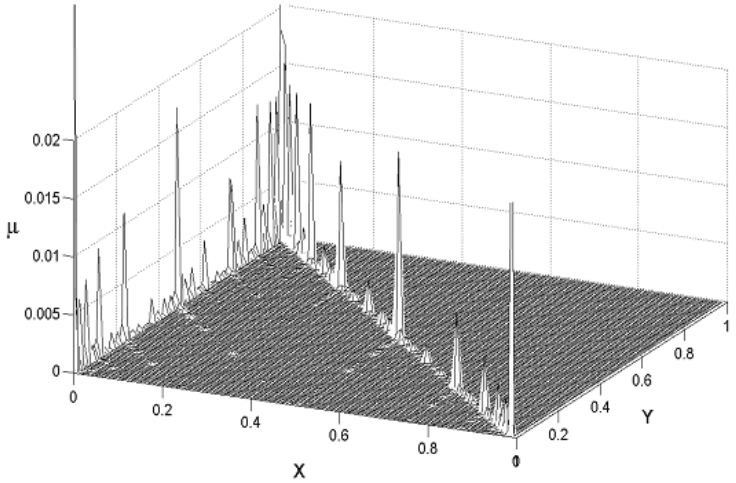

Fig. 13. Toy model measure for active region obtained by means of Chaos Game from empirical one dimensional array $\{t_i\}$.

in the theory of random walks [32]

$$walk = \sum_{all\ \ boxes} (\mu_i - \overline{\mu}), \tag{27}$$

where summation μ_i is made over all boxes of the empirical and model measures, and $\overline{\mu}$ is a mean measure value. For construction of cumulative histograms (figures 14 and 15) 2D distribution of empirical measures were converted to a one dimension array as described above. Then cumulative differences $\mu_i - \overline{\mu}, i = 1, 2, ...$ were calculated. The same procedure was carried out for the RDS model measure, generated by solving the inverse problem.

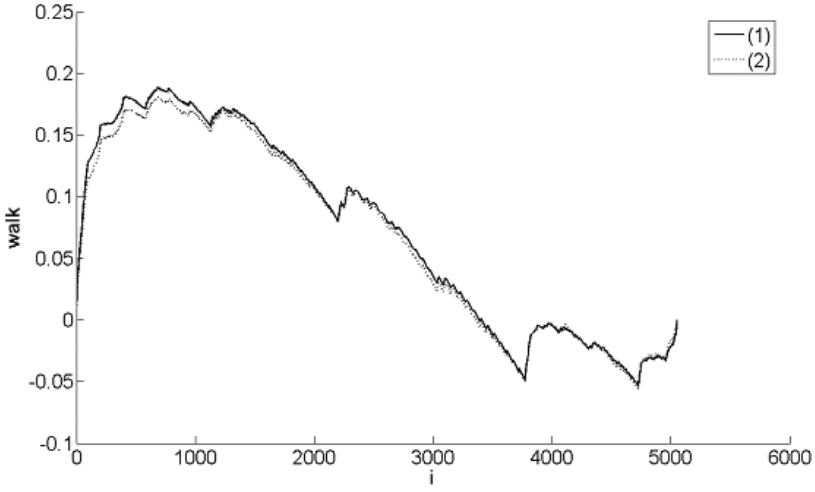

Fig. 14. Cumulative histograms for empirical (1) and RDS model (2) measures corresponding to toy model of background field; i is order number of 1D array.

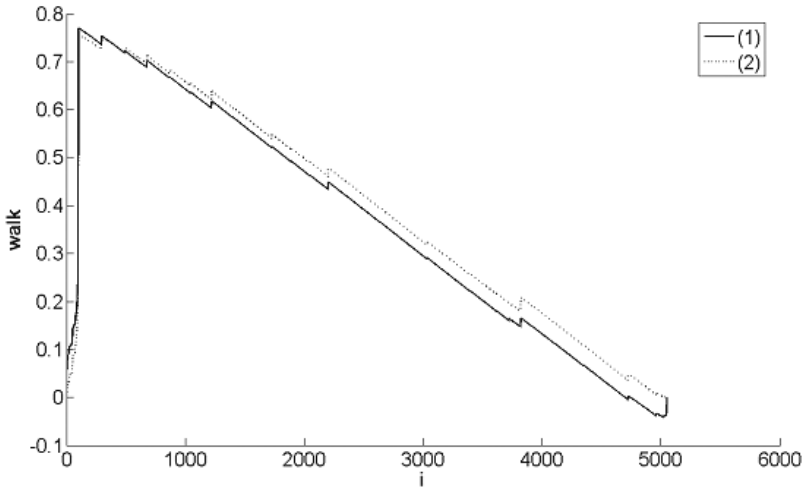

Fig. 15. Cumulative histograms for empirical (1) and RDS model (2) measures corresponding to toy model of active region; i is order number of 1D array.

Figures 14 and 15 show cumulative histograms for RDS model measures in comparison with empirical measures of the background field and active regions, respectively. The curves of the plots for models and the experimental data practically coincide. Hence, obtained estimations of the magnetograms scaling can indeed be obtained from the multifractal properties of the solar magnetic field dynamics.

6 Conclusion

We have investigated the existence of multifractal scaling of Solar magnetic field using MDI magnetograms. To obtain robust estimates of multifractal spectra we applied microcanonic variant of the multifractal formalism based on the Choquet capacity.

Our results make it clear that multifractal spectra can be estimated both for active regions and the background field. It was found that multifractal scaling of background field was stable during approximately 24 hours. Multifractal spectra of active regions have staircase form for the right branch of the spectra and are more erratic.

To verify the reality of multifractal scaling, we constructed a toy model of a chaotic dynamical system, where iterations produce multifractal measure on their own attractor. Measure properties are specified by probabilities of the Markov Iterated Functions System (IFS). We find these probabilities by solving the inverse problem in a frame of IFS theory.

To estimate empirical measure we apply three symbols version of the Chaos Game. Numeric experiments with the Chaos Game were carried out using sampled 256×256 pixels fragments of MDI images of the Sun: fragments of the background field and active regions. Every image matrix was preprocessed, by transforming its elements to the positive values, and normalized. After that matrix was transformed to a 1D array and we obtained time series for the background field and active areas. Their frequency histograms were used to choose thresholds for symbolic transformation.

In order to obtain an empirical estimation of measure produced by RDS dynamics in a frame of toy model, the initial triangle on the plane was divided into boxes, and then relative amount of points inside each box was calculated. In the case of background field, the measure support reproduces the random Sierpinski triangle almost exactly. In the case of active area, the triangle is filled "non-uniformly". The obtained measures were used for the solution of the inverse IFS problem. The found transition probabilities were applied to generate theoretical measure with the help of RDS. Theoretical and empirical measures of toy models were compared by means of cumulative histograms, analogous to those used in the theory of random walks. Thus constructed models fit theoretical and empirical measures of toy models satisfactorily. So, we conclude that obtained estimations of the magnetograms scaling can result from the multifractal properties of the solar magnetic field dynamics.

In contrast to the results of several authors [5–7], we have not found robust time dependence between the AR multifractal spectrum and solar flares. Let us note, that in our previous work [33] we displayed statistical relationship on

a scale ~ 10 years between the *Boulingand-Minkowski dimension* of unipolar region of the large-scale Solar magnetic fields and the so called flare index, which gave roughly the total energy emitted by the flares over a day. However, finding statistically significant precursors of solar flares for time intervals of practical interest (1-2 days) for specified AR is very hard [34–36]. We assume that a precursor displays a specific data structure (or signature), which is typically preceding a flare, allowing for deviations from the given signature. We consider that multifractal spectra of MDI are insufficient to establish precursor of flares, as multifractal spectrum describes only fractal geometry of magnetic turbulence and not the topological structure. Two fractals with the same dimension can be quite different and may be distinguished by a different lacunarity. Consequently, our immediate task is to supplement multifractal characteristics with certain topological indexes.

7 Appendix

σ-ALGEBRA, BOREL SETS AND MEASURES ON R^n [19,37]

A collection $\mathcal{B}$ subset of a set $X \in R^n$ is called a σ-algebra on X iff

(1) $\varnothing, X \in \mathcal{B}$
(2) if $A \in \mathcal{B}$, then $(X - A) \in \mathcal{B}$
(3) if $B_1, B_2, ... \in \mathcal{B}$, then $\cup_{i \in N} \in \mathcal{B}$

A subset $B_i \in \mathcal{B}$ is called a *Borel set*.

We call the *Borel measure* on R^n a function μ which assigns to every subset $A \subset R^n$ a number measure $\mu(A) \in [0, \infty)$ such that

(1) $\mu(\varnothing) = 0$, where $\varnothing$ is empty set;
(2) $\mu(A) \leq \mu(B)$ if $A \subset B$
(3) if $B_1, B_2, ...,$ is a countable (or finite) sequence of Borel sets then

$$\mu(\bigcup_{i=1}^{\infty} B_i) \leq \sum_{i=1}^{\infty} \mu(B_i)$$

with equality if the B_i are disjoint sets, i.e. $B_i \bigcap B_j = \varnothing$ when $i \neq j$.

If $\mu(X) = 1$, then measure is called *normalized* or probabilistic measure.

A finite or countable collection of subsets U_i of R^n is called a δ-cover of the

set $E \subset \cup_{i=1}^{\infty} U_i$. Let E be a set of R^n and $s \geq 0$. For all δ we define

$$H_{\delta}^{s}(E) = inf\{\sum_{i=1}^{\infty} |U_i|^s : \{U_i\} \; is \; a \; \delta - cover \; of \; E\} \tag{28}$$

As δ increases, the class of δ-covers of E is reduced, so this infimum increases and approaches a limit as $\delta \to 0$. Thus we define the s-dimensional *Hausdorff measure* as

$$H^s(E) = lim_{\delta \to 0} H_{\delta}^{s}(E). \tag{29}$$

Hausdorff dimension $d_H(E)$ is defined as

$$d_H(E) = \inf\{s \in R \mid H^s(E) = 0\} = \sup\{s \in R | H^s(E) = \infty\}. \tag{30}$$

The Hausdorff dimension can be calculated in rare cases. In practice, box and capacity dimensions [19] are used instead of the Hausdorff dimension.

Numerical value of the Hausdorff measure can be estimated using some available measure [38]. Let $\mu(A) \geq 0$ be Radon measure, $0 < \lambda < \infty$ and $0 < s \leq n$. And let us suppose that for arbitrary Borel set $A \subset R^n$ and for each point $x \in A$ inequality

$$\limsup_{r \to 0} \frac{\mu[B(x,r)]}{r^s} > \lambda$$

is true. Then there is constant $C = C(s,n)$ such that

$$H^s(A) \leq (C\lambda)^{-1} \mu(A). \tag{31}$$

Push forward measure. The rule for computing the $F \circ \mu(B)$ is very simple. Indeed, let $\{y_l\}$ be set of points of the form $y_l = F(x_k)$ for some k. Then discrete measure $F \circ \mu$ in the sense that there is a finite (or countable) set of points $\{y_l\}$ is

$$w \circ \mu(y_l) = \sum_{F(x_k) = y_l} \mu(x_k) = \mu(F^{-1}(y_l)). \tag{32}$$

There is some problem with this definition if there are infinitely many points x_k which map to the same y_l. However, if the map F is everywhere finite-to-one or linear, there will be no problem.

Hausdorff metric and Monge-Kantorovich-Hutchinson metric [19,30]

The δ-neighbourhood or δ-parallel body, A_δ of a set A is the set of points within distance δ of A, i.e. $A_\delta = \{x||x-y| \leq \delta\}$ for some $y \in A$. Let $\mathcal{H}$ is the class of nonempty compact subsets of X. We may define a metric d_H on $\mathcal{H}$ by

$$d_H(A,B) = inf\{\delta | A \subset B_\delta \; and \; B \subset A_\delta\} \tag{33}$$

It may be shown that d_H satisfies all the requirements for metric and is termed the *Hausdorff metric* on $\mathcal{H}$. The pair $(\mathcal{H}, d_H)$ is complete metric space.

Let (X,d) be a compact metric space and $\mathcal{M}$ denote the set of normalized Borel measures on X. The *Monge-Kantorovich-Hutchinson metric* d_M on $\mathcal{M}$ is defined by

$$d_M(\mu,\nu) = sup\{\int\limits_X f d\mu - \int\limits_X f d\nu\} \tag{34}$$

for all $x, y \in X$ and $\mu, \nu \in \mathcal{M}(X)$. Here the supremum is taken for all continuous function $f : X \to R$ such, that $|f(x) - f(y)| \leq d(x,y)$, and the integrals in (34) can be understood as $\mu(x)$-weighted value of f on intervals $\{I_k\} \in X$ i.e.

$$\int\limits_X f(x) d\mu(x) \approx \sum_{I_k} f(x_k)\mu(I_k), \tag{35}$$

References

[1] A. Brandenburg, K. Subramanian. Astrophysical magnetic fields and nonlinear dynamo theory *Physics Reports* **417** 1-209 (2005)

[2] M. K. Georgoulis. Turbulence in the Solar Atmosphere: Manifestations and Diagnostics via Solar Image Processing *Solar Physics* **228** 5 (2005)

[3] J. K. Lawrence, A. C. Cadavid, A. A. Ruzmaikin. On the multifractal distribution of Solar magnetic fields *Astrophys. J.* **465** 425-435 (1996)

[4] R. Neil, Jr. Sheeley. Surface Evolution of the Sun's Magnetic Field: A Historical Review of the Flux-Transport Mechanism *Living Rev. Solar Phys.* **2** 5 (2005)

[5] N. Meunier. Fractal Analysis of Michelson Doppler Imager Magnetograms: A Contribution to the Study of the Formation of Solar Active Regions *Astrophys. J.* **515** part 2 801-811 (1999)

[6] B. Stark, M. Adams, et al. Evaluation of Two Fractal Methods for Magnetograms Image Analysis *Solar Phys.* **174** No.1-2. 297-309 (1997)

[7] V. I. Abramenko, V. B. Yurchyshyn, et.al. Scaling Behavior of Structure Functions of the Longitudinal Magnetic Field in Active Regions on the Sun *Astrophys. J.* **577** No.1 487 (2002)

[8] R. T. J. McAteer, P. T. Gallagher, J. Ireland. Statistics of Active Region complexity: a large-scale fractal dimension survey *Astrophys. J.* **631** 628 (2005)

[9] I.I. Salakhutdinova, A.A. Golovko. The variations of the scaling parameters of the structure functions in solar active regions at the pre-flare stage. *Solar Physics* **225** 59 (2004)

[10] S.Criscuoli, M. P. Rast, I. Ermolli, and M. Centrone. On the reliability of the fractal dimension measure of solar magnetic features and on its variation with solar activity *Astronomy and Astrophysics* **461** 331 (2007)

[11] J. Mach, F. Mas, F. Sagués. Two representations in multifractal analysis *J. Phys, A: Math. Gen.* **28** 5607-5622 (1995)

[12] A. Arneodo, E. Bacry. J. F. Muzy. The thermodynamics of fractals revisited with wavelets *Physica A* **213** 232 (1995)

[13] J. Levy-Vehel, R. Vojak. Multifractal analysis of Choquet capacities: Preliminary Results Advances. *Applied Mathematics* **20** 1 (1998).

[14] N. G. Makarenko, L. M. Karimova, S. A. Mukhamejanova, I. S. Knyazeva. Iterated Function System and Markovian prediction of time series *Applied Nonlinear Dynamics* **14** No.6 3 (2006) (in Russian)

[15] J. A. Wanliss, V. V. Anh, et al. Multifractal modeling of magnetic storms via symbolic dynamics analysis *J.Geophys.Res.* **110** AO814 (2005)

[16] B. Forte, E. R. Vrscay. Solving the inverse problem for function/image approximations using iterated function systems. *Fractals* **2,3** 325, 346 (1994)

[17] R. Riedi, I. Scheuring. Conditional and relative multifractal spectra *Fractals* **5** 153 (1997)

[18] D. Harte. Multifractals *CRC Press* 247p. (2001)

[19] K. Falconer. Techniques in fractal geometry. *John Wiley & Sons* 256p. (1997)

[20] T. C. Halsey, M. H.Jensen, L. P. Kadanoff et all. Fractal measures and their singularities: the characterization of strange sets *Phys.Rev.A.* **33** 1141 (1968).

[21] O. Pont, A. Turiel, et al. Application of the microcanonical multifractal formalism to monofractal systems *Physical Review E* **74** 061110(1)-(13) (2006)

[22] A.Turiel, C. J.Perez-Vicente, et al. Numerical methods for the estimation of multifractal singularity spectra on sampled data: a comparative study *J. Comput. Physics* **216** 362-390 (2006)

[23] J. Levy-Vehel. Introduction to the multifractal analysis of images *NATO advanced study institute on fractal image encoding and analysis, Trondheim, NORVEGE (08/07/1995),Springer-Verlag* **159** 299 (1998)

[24] J. Levy-Vehel, J. P. Berroir, Image analysis through multifractal description in *Fractals in the Natural and Applied Sciences, ed. M. M. Novak, North-Holland* **A-41** 261 (1993)

[25] http://soi.stanford.edu/magnetic/index5.html

[26] http://www.irccyn.ec-nantes.fr/hebergement/FracLab/

[27] G. Froyland. Extracting dynamical behaviour via Markov models in *Nonlinear dynamics and statistics* A.I. Mees ed. Birkhauser 283 (2001)

[28] E. R. Vrscay. From fractal image compression to fractal-based methods in mathematics *Fractals in Multimedia*. ed. by M.F. Barnsley, D. Saupe, E.R. Vrscay. New York: Springer-Verlag (2002).

[29] Z. G. Yu, V. V. Anh, et al. Chaos game representation of the Dst index and prediction of geomagnetic storm events *Chaos, Solitons and Fractals* **31** 736-746 (2007)

[30] M. Barnsley. Fractals everywhere. *Orlando: Academic Press* 531p. (1988).

[31] J. H. Jeffrey. Chaos game representation of gene structure *Nucleic Acids Research* **18** No.8 2163-2170 (1990)

[32] R.Metzler, J.Klafter. The random walk's guide to anomalous diffusion: a fractional dynamic approach. *Physical Reports* **339** 1-72 (2000).

[33] N. G. Makarenko, L. M. Karimova, M. M. Novak. Dynamics of Solar magnetic fields from synoptic charts *Emergent Nature. Patterns, Growth and Scaling in the Sciences.* M. M. Novak editor. World Scientific 197-207 (2001)

[34] G. Barnes, K. D. Leka et al. Probabilistic forecasting of solar flares from vector magnetogram data. *Space Weather* **5** SO9002 (2007)

[35] K. D. Leka, G. Barnes Photospheric magnetic field properties of flaring versus flare-quiet active regions. I. Data, General approach, and sample results. *Astrophys. J.* **595** 1277-1295 (2001)

[36] S. Hallerberg, H. Kantz. Influence of the event magnitude on the predictability of an extreme event. *Phys. Rev. E* **77**, 011108 (2008)

[37] G.Edgar. Measure, Topology, and Fractal Geometry. *Springer* 293p.(2008)

[38] W.P.Zieman. Weakly differentiable functions. *New York: Springer-Verlag* 370p. (1989).